Impact of Urban Cover Fraction on SMOS and SMAP Surface Soil Moisture Retrieval Accuracy

Nan Ye, Jeffrey P. Walker, *Fellow, IEEE*, Christoph Rüdiger, *Senior Member, IEEE*, Dongryeol Ryu, *Member, IEEE*, and Robert J. Gurney

***Abstract*—Both the European Space Agency's soil moisture and ocean salinity (SMOS) mission and the National Aeronautics and Space Administration's soil moisture active passive (SMAP) mission employ *L*-band (1.413 GHz) radiometers to observe brightness temperatures at ∼40-km spatial resolution to subsequently derive global soil moisture every two to three days with a target accuracy of 0.04 m^3/m^3. However, the man-made structures that dominate urban areas in many of the SMOS and SMAP radiometers pixels may confound the interpretation of their radiometric observations if not taken into account, and thus, degrade the soil moisture retrieval accuracy. This paper investigates the effect that urban areas are expected to have on the SMOS and SMAP soil moisture retrieval accuracy using experimental data from the Australian airborne field campaigns performed over the past six years. Taking the total radiometric error budgets for the SMOS (3.95 K) and the SMAP (1.3 K) missions as conservative benchmarks for radiometric "error" that can be tolerated to achieve the 0.04 m^3/m^3 target accuracy, urban fraction thresholds of 6.6% and 2.2% were obtained for the SMOS and SMAP pixels, respectively, under warm dry (soil moisture < 0.15 m^3/m^3) conditions, increasing to 16.8% and 5.2% under cold and/or wet conditions. These results have been extrapolated globally, assuming that the microwave behavior of the cities analyzed here is representative of those elsewhere, to identify the SMOS and SMAP pixels that are expected to be adversely affected by urban areas if not explicitly taken into account in retrieval algorithms.**

***Index Terms*—Passive microwave, remote sensing, soil moisture, urban fraction.**

I. Introduction

Soil moisture plays a significant role in atmosphere and earth-surface interactions since it controls the rainfall partitioning into infiltration and runoff [1], influences the evaportranspiration and vegetation photosynthetic rate [2], and impacts the activities of soil microorganisms [3]. Thus, knowing the distribution of soil moisture with adequate temporal and spatial resolution is required by many disciplines, including hydrology, meteorology, and agriculture [4]. However, due to its variability in time and space, soil moisture is difficult to be measured using monitoring station networks at regional and global scales [5]–[10].

During the last three decades, passive microwave remote sensing at low-frequency bands has been widely acknowledged as the most promising technique to measure spatial distribution of water content in the top ∼5 cm of soil, due to its direct relationship to the soil dielectric constant, its ability to penetrate clouds, and its reduced sensitivity to vegetation and surface roughness [11]–[14]. The first soil moisture dedicated satellite, the soil moisture and ocean salinity (SMOS) mission of Europe Space Agency, was launched on November 2, 2009 carrying a two-dimensional interferometric radiometer to measure microwave emissions from the earth's surface at *L*-band (1.413 GHz) [15]. By inverting radiative transfer models, these brightness temperature observations are used to determine the surface soil moisture content with a target accuracy of ∼0.04 m^3/m^3 [16]. In addition, the National Aeronautics and Space Administration's soil moisture active passive (SMAP) mission was launched on January 31, 2015 consisting of an *L*-band real aperture radiometer [17].

Based on the current level of antenna technology, the best spatial resolution that can be directly achieved at *L*-band by both the SMOS and SMAP radiometer approaches is on the order of 40 km [15], [17]. At such a coarse scale, urban areas are present within many SMOS and SMAP pixels globally, especially over heavily populated continents like Europe. A key concern in relation to urban areas is the adverse effects of man-made emitters, known as radio frequency interference (RFI), on the quality of passive microwave observations. Consequently, a great effort has been made to switch OFF RFI sources over Europe, China, South Asia, and the Middle East since SMOS was launched [18]. However, after all RFI sources have been removed [19], [20], the soil moisture retrieval accuracy target of 0.04 m^3/m^3 may still not be achieved over urban areas unless the effects of man-made structures themselves are explicitly taken into account, since the microwave behavior of man-made structures is significantly different from that of the natural targets [21]. The microwave contribution of urban areas to spaceborne radiometer observations has not been taken into account in the current soil moisture retrieval models due to the lack of understanding of the microwave behavior of urban areas, and it is this microwave contribution from man-made structures that forms the focus of this study. As RFI is not considered

Manuscript received September 10, 2018; revised May 29, 2019; accepted June 28, 2019. This work was supported by the Australian Research Council within the framework of the MoistureMap Project DP0879212. *(Corresponding author: Nan Ye.)*

N. Ye, J. P. Walker, and C. Rüdiger are with the Department of Civil Engineering, Monash University, Clayton, VIC 3800, Australia (e-mail: ye.nan@monash.edu; jeff.walker@monash.edu; chris.rudiger@monash.edu).

D. Ryu is with the Department of Infrastructure Engineering, University of Melbourne, Parkville, VIC 3010, Australia (e-mail: dryu@unimelb.edu.au).

R. J. Gurney is with the Department of Meteorology, University of Reading, Reading RG6 6AH, U.K. (e-mail: r.j.gurney@reading.ac.uk).

Color versions of one or more of the figures in this paper are available online at http://ieeexplore.ieee.org.

Digital Object Identifier 10.1109/JSTARS.2019.2929482

further in this paper, the term urban effects should be interpreted herein to mean the influences on microwave radiometric observations from the man-made structures that dominate urban areas.

According to Schneider *et al.* [22], less than 0.5% of the world's land mass is classified as urban, suggesting that most of the SMOS and SMAP pixels will have either no or insignificant urban contribution to brightness temperature observations. However, urbanization is not homogeneously spread across the globe, and so urban areas are likely to have significant contributions to brightness temperature observations over the SMOS and SMAP pixels once the fraction of urbanized areas in a pixel exceeds some threshold, resulting in soil moisture retrieval errors exceeding the aforementioned target accuracy ($\sim$0.04 m^3/m^3) of these missions. Consequently, it is important to know this urban fraction threshold, and thus identify the SMOS and SMAP pixels with a potentially large urban impact on soil moisture retrieval, in order for them to be better flagged or a brightness temperature correction applied during the soil moisture retrieval process. This paper fills that niche.

To date, there is little knowledge about how urban areas impact on soil moisture retrieval with most existing understanding based on the simulation results from a limited number of synthetic studies (e.g., [16], [23]); no studies have been undertaken using real microwave observations. In the SMOS algorithm theoretical basis document [16], the urban area is assumed to behave as a very dry bare soil or rock whose dielectric constant is suggested to be $5.7 - j \times 0.074$. Based on model simulations under a range of conditions, a rock cover fraction threshold of 11% was derived for the SMOS soil moisture target accuracy of 0.04 m^3/m^3, which was assumed to be applicable to urban areas. Similarly, Loew [23] derived an urban fraction threshold of 15%–20% from model simulations conducted over the Upper Danube catchment in southern Germany, assuming that urban areas behave like a very dry bare soil with a low and fixed dielectric constant and high surface roughness. Consequently, this paper here examines the previously reported urban fraction thresholds, using real data acquired from the three Australian field experiments. Subsequently, these thresholds are used to identify the SMOS and SMAP pixels where the target soil moisture retrieval error will likely be exceeded as a result of urban-induced error.

The objectives of this study are as follows.

1) Investigate the relationship between urban cover fraction and *L*-band microwave brightness temperature using airborne observations.
2) Obtain thresholds of urban cover fraction that the presence of urban can be ignored in soil moisture retrieval.
3) Demonstrate the SMOS and SMAP pixels globally, where the soil moisture retrievals accuracy may be adversely affected if the presence of urban areas is not accounted for.

In this study, the SMOS and SMAP radiometric error budgets of 3.95 K [15] and 1.3 K [17] were used as the brightness temperature error budgets to be met in order to achieve the target soil moisture retrieval accuracy of 0.04 m^3/m^3. Consequently, these limits were used to define the urban-induced brightness temperature deviation that could be tolerated from what would otherwise have been made for a natural landscape; a somewhat conservative assumption that the entire error budget could be attributed to urban effects alone. The urban fraction thresholds obtained using these experimental data were then used to identify the SMOS and SMAP pixels globally where the soil moisture retrieval error will potentially exceed the target accuracy as a result of man-made structures. A key assumption of this extrapolation is that the Australian cities located in the study areas represent the microwave response of cities worldwide.

II. Datasets and Study Areas

A. Airborne Microwave Brightness Temperature Observations

Airborne brightness temperature observations and monitoring station data collected during the three Australian airborne field experiments were used to establish the relationship between urban-induced brightness temperature error and urban fraction. The National Airborne Field Experiment in 2006 (NAFE'06 [24]), Australian Airborne Cal/val Experiments for SMOS (AACES-1 and AACES-2 [25]) were conducted in the Murrumbidgee River catchment in southeastern Australia during the Australian summers of 2006 (October 29, 2006–November 20, 2010) and 2010 (January 18, 2010–February 21, 2010), and the winter of 2010 (September 8, 2010–September 26, 2010), respectively. Fig. 1 shows the location of the study areas, monitoring stations, studied cities, the SMAP Equal-Area Scalable Earth (EASE) 36-km grid, and the SMOS overlapped footprints which are reconstructed to $\sim$43-km resolution on the SMOS discrete global grid (DGG).

In this study, data collected over 13 sampling days across the eight SMOS and SMAP sized areas were analyzed (see Table I). The brightness temperature over seven medium-to-large cities across the catchment (see Table II) was measured using the polarimetric *L*-band multibeam radiometer (PLMR) mounted on a scientific aircraft. The PLMR is a multibeam dual-polarized (vertical and horizontal) radiometer operating at 1.413 GHz with a bandwidth of 24 MHz. In push broom configuration, the PLMR has six across-track beams with view angles of 7°, 21.5°, and 38.5° to both the sides of the aircraft. Each observation has a beam width of 17° along-track and 14° across-track. Before and after each flight, the PLMR was calibrated using the sky (cold target) and a temperature-recorded blackbody box (warm target). In addition, the calibration of the PLMR was confirmed during each flight using brightness temperature observations over a calibration lake having *in situ* measurements of water temperature and salinity collected by a floating monitoring station. After pre and postflight calibration, the PLMR has an overall accuracy of better than 2 K [26]. During each sampling day, microwave emissions of the entire patch were measured across a $\sim$5-h flight window at an altitude of $\sim$3000 m above the ground level, yielding a ground resolution of $\sim$1 km. Moreover, the first $\sim$12 km of the first flight line was repeated at the end of each flight in order to capture the temporal variation of microwave emission during the flight. A small bias was observed for the repeated flight line, which was subsequently removed.

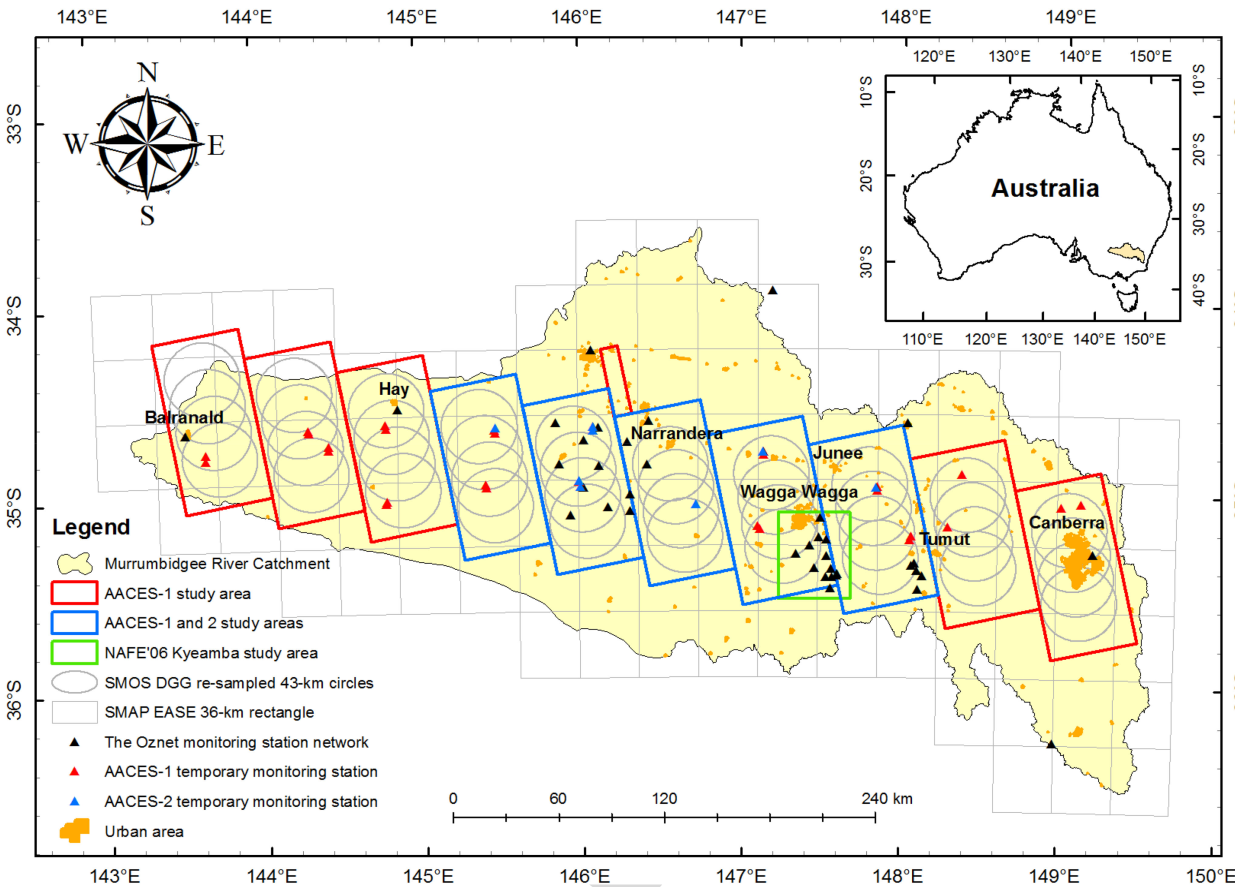

Fig. 1. Location of the Kyeamba study area of the NAFE'06, ten flight patches of the AACES-1 and five flight patches of the AACES-2 in the Murrumbidgee River catchment in south-eastern Australia (inset). The SMOS DGG resampled pixels within each AACES flight patch, the SMAP EASE pixels over the entire catchment, and the long-term soil moisture network sites (OzNet) and temporary monitoring stations of AACES campaigns are also shown.

TABLE I
LIST OF FLIGHTS MADE OVER CITIES ACROSS THE MURRUMBIDGEE RIVER CATCHMENT

Dataset	Sampling date	Flight patch	Reference time (local)	Studied city
NAFE'06	30th Oct. 2006	Kyeamba	12.00pm	Wagga Wagga
	6th Nov. 2006	Kyeamba	12.00pm	Wagga Wagga
	20th Nov. 2006	Kyeamba	12.00pm	Wagga Wagga
AACES-1	22nd Jan. 2010	1	6:00 am	Balranald
	28th Jan. 2010	3	6:00 am	Hay
	12th Feb. 2010	6	6:00 am	Narrandera
	10th Feb. 2010	7	6:00 am	Wagga Wagga
	15th Feb. 2010	8	6:00 am	Junee
	18th Feb. 2010	9	6:00 am	Tumut
	18th Feb. 2010	10	6:00 pm	Canberra
AACES-2	19th Sep. 2010	6	6:00 am	Narrandera
	21st Sep. 2010	7	6:00 am	Wagga Wagga
	22nd Sep. 2010	8	6:00 am	Junee

TABLE II
MAIN FEATURES OF THE STUDIED CITIES. THE CENSUS DATA WERE RETRIEVED FROM [27]

Studied city	Population density in 2010 [km^{-2}]	Manmade structures derived from the LUNSW [km^2]	Industrial ratio [-]	Residential ratio [-]	Others ratio [-]
Balranald	0.1	1.61	0.27	0.73	0.00
Hay	0.3	2.72	0.31	0.65	0.04
Narrandera	1.5	4.90	0.30	0.66	0.04
Wagga Wagga	13.2	37.51	0.24	0.68	0.08
Junee	3.1	4.22	0.23	0.63	0.14
Tumut	2.5	4.81	0.25	0.69	0.06
Canberra	443.5	170.31	0.11	0.89	0.00

B. Airborne Data Preprocessing

The temporal variation of brightness temperatures due to changes in the physical-surface temperatures during the flight was corrected by multiplying each brightness temperature observation with the ratio between effective soil temperature at the current time and that at a fixed reference time (generally the mid duration of the flight). The effective soil temperature was calculated using the time series of top ∼5 cm soil moisture and soil temperature at 2.5-cm and 40-cm depth, collected by monitoring stations within each patch using the method presented in [28]. In the NAFE'06 dataset, the brightness temperature observations were corrected to 12 noon (local time) using data from the OzNet monitoring station network [www.oznet.org.au; 29]. In the AACES-1 and -2, the 6 A.M. and 6 P.M. SMOS ascending and descending overpass times were used as the reference time, with data from temporal monitoring stations installed during the campaigns used for the temporal correction. Using this correction technique, the bias of the brightness temperature observations between the repeated flights reduced to less than 1 K, which is insignificant in comparison with the brightness temperature difference between the urban and natural soil areas.

The angular difference of the brightness temperature observations was corrected by normalizing the observations to 38.5° using the cumulative distribution function (CDF)-based normalization method of presented in [42]. The method normalizes multiangle observations to a reference angle by matching the CDF of each incidence angle to that of the reference angle. This approach assumes that the brightness temperature variations viewed by each incidence angle has the same statistical properties, and has been shown to result in normalization errors for individual observations as low as ∼1 K. Consequently, the normalization error for scene-averaged brightness temperatures is assumed to be negligible.

C. Urban Distribution Data

The urban area is a combination of man-made structures (e.g., buildings and roads) and natural land surfaces (e.g., parks and gardens), and these man-made structures are hypothesized to have a distinct microwave response from natural soil targets that will adversely affect soil moisture retrieval if not explicitly taken into account. To quantify the impact of the urban areas on the observed radiometric response, man-made structures in the Murrumbidgee River catchment were identified using the land use New South Wales [LUNSW; 43] product due to its high resolution of better than 15 m. The LUNSW is a regional land use dataset mapped in polygon format over the state of New South Wales (NSW), Australia. The land use classification and mapping was undertaken directly from the satellite imagery and aerial photography with assistance from existing datasets, local knowledge, and field checking. According to an independent verification conducted by checking the satellite imagery and aerial photographs, the LUNSW has a positional accuracy of 50 m and an attribute accuracy of 92%–99% [43]. In the LUNSW, urban land use is classified as a combination of 29 subclasses, including industrial/commercial, residential, recreational, landfill, and other urban facilities. The subclasses of urban class in the LUNSW were regrouped into man-made structures dominated by built-up environment and rural residential dominated by natural areas. Consequently, open space in urban areas is explicitly accounted for when determining the fractions of man-made structures and rural residential.

To identify the global SMOS and SMAP pixels with urban-induced brightness temperature contribution in excess of the respective error budgets, a global urban map with appropriate spatial resolution and accuracy is required. There are currently ten different global urban and urban-related land surface maps available, as listed in Table III. Different types of data were used in the classifications; thus, they differ in terms of their definition of "urban," spatial resolution, and accuracy. For example, the urban maps that are derived from census data and night-time lights relate to population and income level, while the urban maps derived from multispectral data relate more to built-up areas [44], [45]. Compared with natural land surfaces, the difference of microwave behavior of urban areas is due to the distribution of man-made structures, not population or other factors. Consequently, only the maps that define urban as built-up or impervious area and have a spatial resolution better than 1 km were considered in this study (i.e., Maps 1–6 in Table III).

The accuracies of these maps were assessed in [22] by comparing urban maps over 140 randomly sampled cities globally, by manual interpretation using 30-m Landsat data. The assessment result showed that the MODerate resolution Imaging Spectroradiometer (MODIS) 500-m urban land cover dataset had the highest accuracies in classified urban pixel (93%) and in estimated city size ($R^2 = 0.90$). The MODIS 500-m is a global urban land use map with a spatial resolution of 500 m, generated using a supervised decision tree algorithm based on MODIS Collection 5 data between 2001 and 2002. In the MODIS 500-m dataset, urban areas are defined as pixels having more than 50% built-up land surface with a minimum size of 1 km^2 [22].

D. Calculation of Urban Cover Fraction

To apply the urban fraction threshold derived from the LUNSW globally, a global urban map was required to calculate the urban fraction of the global SMOS and SMAP pixels, which should be classified based on man-made structures and consistent with the LUNSW at the scales of SMOS and SMAP. Consequently, the cover fractions of man-made structures and urban areas in the SMOS DGG pixels with approximately 43-km resolution and SMAP EASE 36-km pixels over the Murrumbidgee River catchment were calculated using the LUNSW and each of the global urban maps, respectively. Fig. 2 shows the urban fractions calculated using each of the global Maps 1 to 5 against the cover fractions of man-made structures using the LUNSW over the corresponding SMOS and SMAP pixels in the Murrumbidgee catchment. Due to its lower resolution compared to its upgraded version (MODIS 500-m dataset), the MODIS 1-km urban land use dataset (Map 6) was discarded in the comparison. It is clear that the GRUMP, GLC2000, and GlobCover datasets overestimate the urban area as compared with man-made structures in the LUNSW, while the ISA dataset

TABLE III
KEY CHARACTERISTICS OF EXISTING GLOBAL URBAN MAPS (ADAPTED FROM [22])

ID	Abbreviation	Map	Factor defining urban or urban-related feature	Resolution	Main source of data	Urban fraction ratio to the LUNSW
1	GLC2000 [30]	Global Land Cover 2000	Artificial surfaces and associated areas	~1 km	SPOT-Vegetation, Nighttime lights data	1.36
2	GlobCover [31, 32]	GlobCover v2.2	Artificial surfaces and associated areas	~300 m	MERIS	1.37
3	GRUMP [33]	Global Rural–Urban Mapping Project	Urban extent	~1 km	VMAP, census data, Nighttime lights maps	3.68
4	ISA [34]	Global Impervious Surface Area	Impervious surface area	~1 km	Landscan, Nighttime lights data Landset data for training	0.31
5	MODIS 500-m [22]	MODIS Urban Land Cover 500 m	Urban and built-up areas	~500 m	MODIS and Landsat-based map for training and assessment.	0.93
6	MODIS 1-km [35]	MODIS Urban Land Cover 1 km	Urban and built-up areas	~1 km	MODIS, Landsat-based map for training and assessment and LITES	-
7	HYDE [36, 37]	History Database of the Global Environment v3	Urban and built-up areas	~10 km	Landscan, UN census data, city gazetteers	-
8	VMAP [38]	Vector Map Level Zero	Population	1:1 million	Aeronautical charts, maps	-
9	Lights [39, 40]	Nighttime Lights v2	Nighttime Lights	~1 km	DMSP-OLS dataset	-
10	LandScan [41]	LandScan 2005	Population	~1 km	Geocover maps, VMAP0, MODIS 1-km, Landsat, census data, high-resolution imagery	-

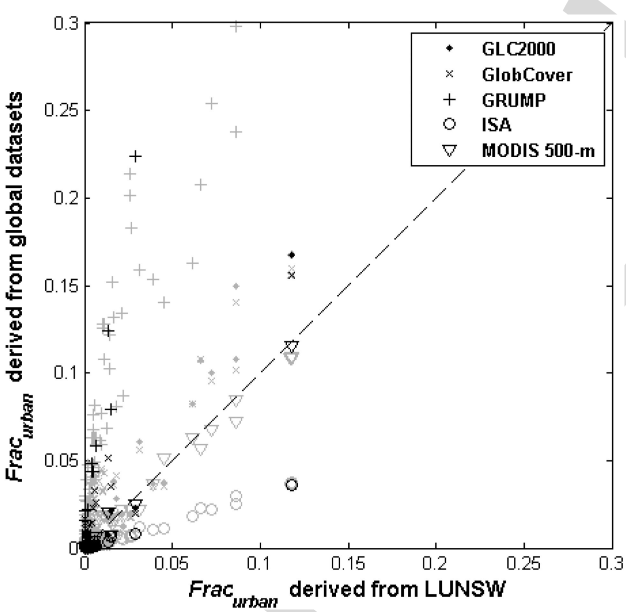

Fig. 2. Comparison between the LUNSW and MODIS 500-m in terms of urban fraction of the SMOS DGG resampled pixels (gray symbol) and the SMAP EASE 36-km pixels (black symbol) over the Murrumbidgee River catchment.

provides an underestimate. The mean ratio of pixel urban fraction calculated using each of Maps 1–5 to the cover fraction of man-made structure derived from the LUNSW is listed in the last column of Table III, confirming that the MODIS 500-m has the best agreement with man-made structures in the LUNSW, having an urban extent ratio of 0.93. In the context of 11%–20% urban fraction threshold obtained from the previous simulation studies [16], [23], the difference between the LUNSW man-made structures and MODIS 500 m is approximately 1% at the SMOS and SMAP scale, which was considered to be negligible. Consequently, the MODIS 500-m urban map was selected for calculating urban fraction of all the SMOS and SMAP pixels globally. It needs to be noted that the temporal variation of urban extent from 2002 (for MODIS 500-m) to 2010 (for AACES) was ignored.

III. METHODOLOGY

The impact of urban fraction on soil moisture retrieval was investigated in four steps, as illustrated in Fig. 3.

Step 1. Prepare airborne brightness temperature data and land cover maps for a range of urban cover fractions: The airborne brightness temperature observations at 1-km resolution were aggregated to larger scales in order to simulate the SMOS and SMAP scenes with a range of urban fraction ($Frac_{\mathrm{urban}}$), and the simulated brightness temperature data were calculated for the urban-free part (TB_{nonurban}) and entire scene (TB_{all}) by averaging 1-km brightness temperature observations over urban-free pixels and all pixels within the corresponding scene, respectively. To achieve a wide range of scene urban fraction, a 40-km rectangle window was moved within the study area. However, according to the size of the studied cities as listed in Table II, the maximum cover fractions at 40 km are less than 11%–20% urban fraction threshold obtained from the simulation studies presented in [16] and [23]. To obtain results for a greater range of urban fraction thresholds,

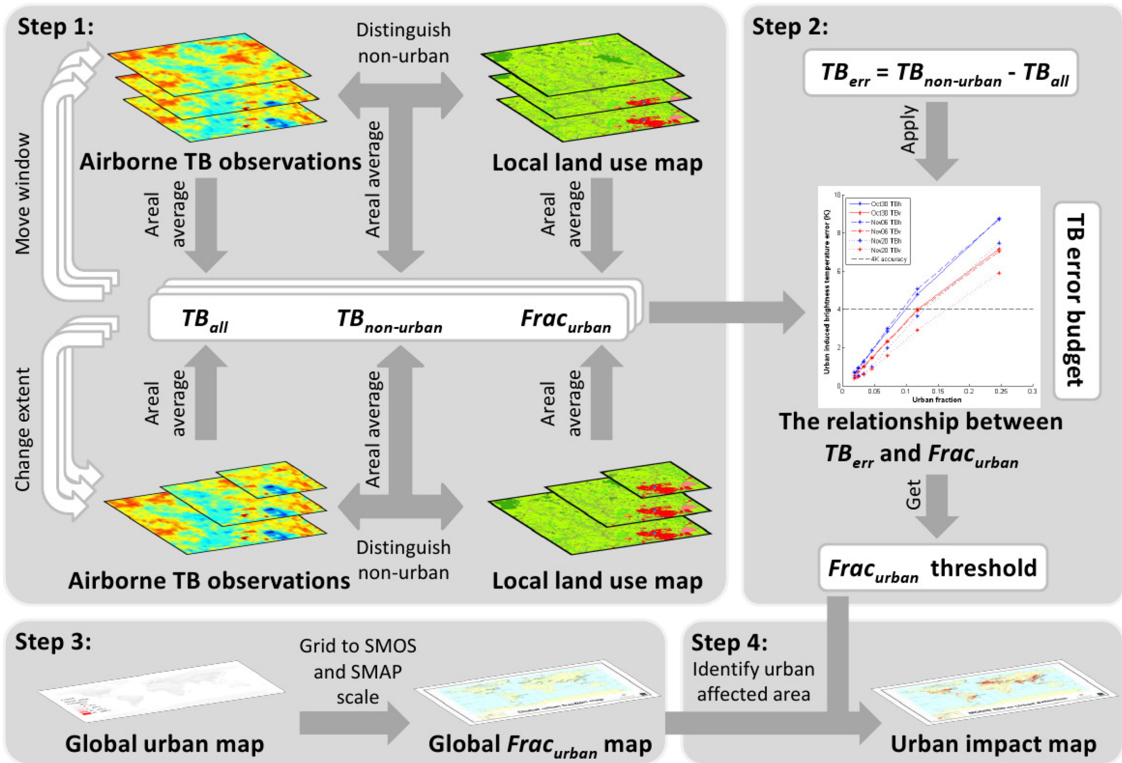

Fig. 3. Schematic flowchart of methodology.

the scene was centered on the studied cities and the window size gradually decreased, assuming that the brightness temperature integrated from smaller scales is the same as that at the SMOS and SMAP scales [46]. The recategorized LUNSW dataset was used to determine the urban fraction and identify the urban-free brightness temperature pixels in the 1-km PLMR data.

Step 2. Investigate the relationship between urban cover fraction and brightness temperature: The SMOS and SMAP radiometric sensitivity of 3.95 and 1.3 K [15], [17] were used as brightness temperature error budgets to determine the thresholds for urban cover fraction in the SMOS and SMAP pixels, below which an urban-induced brightness temperature contribution can be ignored as a part of the overall instrument uncertainty. This urban-induced brightness temperature "error" (TB_{err}) is defined hereafter as the difference between TB_{nonurban} and TB_{all}, which represent spaceborne brightness temperature observations both with and without accounting for the contribution of urban area, respectively. Based on the relationship between $Frac_{\mathrm{urban}}$ and TB_{err}, urban fraction thresholds were derived for the SMOS and SMAP brightness temperature error budgets, respectively, ignoring the differences of the pixel shape and size between the SMOS and SMAP.

Step 3. Calculate urban cover fraction of the global SMOS and SMAP pixels: The MODIS 500-m urban land use map was used to calculate urban fraction of the SMOS and SMAP pixels globally. The SMOS mission uses the Icosahedral Snyder equal area (ISEA)-based Aperture 4 hexagon DGG in Resolution 9, which maps the earth surface into $\sim$2.6 $\times$ 10^6 hexagon cells with an equal area of $\sim$194 km^2 and an equal distance of $\sim$15 km between the center points of adjacent cells [47]. Although the center points of SMOS $L1$ and $L2$ data are fixed on the DGG points, the size and orientation of the pixels vary for the $\sim$500 km partly overlapped SMOS scenes in the Murrumbidgee River catchment, and the SMOS footprints were simplified to overlapping circles with a diameter of 43 km, being the average SMOS pixel size [15] centered on the SMOS DGG points. Similarly, the EASE Grid 2.0 [48] was used for application to SMAP. The EASE grid is defined in three projections: Northern and southern hemispheres (Lambert azimuthal equal-area projections) and full global (a cylindrical equal-area projection with standard parallels at $\pm$30°). The global EASE grid at 36-km resolution has been selected for the SMAP radiometer products. Consequently, the urban fractions ($Frac_{\mathrm{urban}}$) in the SMOS DGG resampled 43-km circles and the SMAP 36-km EASE grid were calculated using the MODIS 500-m urban land surface map.

Step 4. Identify the urban affected pixels of SMOS and SMAP: The urban fractions of SMOS and SMAP pixels at global scale were then used together with the thresholds obtained for the SMOS and SMAP radiometric sensitivities obtained in Step 2, and then applied

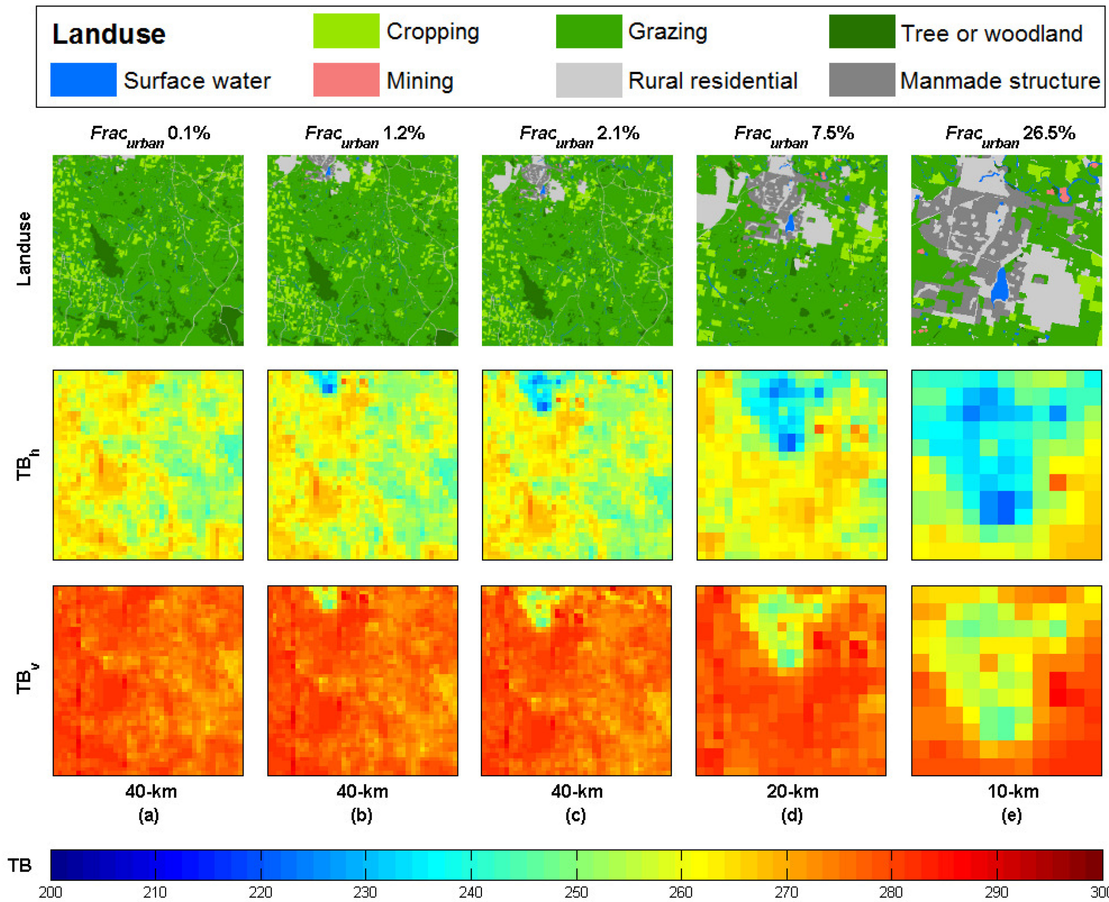

Fig. 4. LUNSW and dual-polarized brightness temperature (TB_h and TB_v) maps at 38.5° incidence angle for scenes with different urban fractions over the city of Wagga Wagga on November 6, 2006.

to the urban fractions obtained in Step 3 to produce global maps of urban effected pixels. As one of the first studies on urban effect, this study started from a simplified scenario. A key assumption of this step is that the microwave behavior of the studied cities represents that of urban areas worldwide.

IV. Results

A. Simulated Urban Effects Scenarios

A range of scenes were simulated for the SMOS and SMAP pixels by moving the window of a scene at SMOS and SMAP scales within the study area, and by reducing the extent of a scene centered on the studied cities. As an example, Fig. 4 shows the land use as well as horizontally and vertically polarized brightness temperature maps of scenes within the Kyeamba study area using airborne observations collected on November 6, 2006 during the NAFE'06 campaign. According to the re-categorized LUNSW classification, this area is dominated by cropping and grazing land, intermixed with man-made structures, rural residential, trees, water bodies, and mining area. Compared to brightness temperature maps, the nonsoil targets have a distinctive microwave response. The urban area and open water have ~30 K lower brightness temperature than the surrounding grass and cropping land surfaces, while the brightness temperatures of trees were ~10 K higher. The impact of forest and water bodies was removed by discarding the 1-km brightness temperature pixel with more than 5% cover fraction of forest and/or water bodies.

Fig. 4 has a good spatial agreement between the man-made structures and very low brightness temperature pixels, implying a good correlation between recategorized man-made structures and urban-affected brightness temperature pixels. From Column (a) to (c) in Fig. 4, a 40 × 40-km^2 scene was moved from the southernmost part of the study area toward the studied city (Wagga Wagga) in the north, with the urban fraction ($Frac_{\mathrm{urban}}$) of the scenes varying from 0.1% when the studied city was almost outside of the scene to 2.1% when the studied city was fully in the scene. To obtain a higher range of urban fractions, the scene was positioned over the urban area and the extent of the scene reduced from 40 km to 20 km and then to 10 km [Columns (c)–(e)], resulting in urban fractions up to 26.5% in this example.

B. Relationship Between Urban Cover Fraction and Urban-Induced Error in Brightness Temperature

The brightness temperature observations of all pixels in each scene were then averaged to TB_{all}, and the equivalent urban free brightness temperature estimated as TB_{nonurban} by discarding

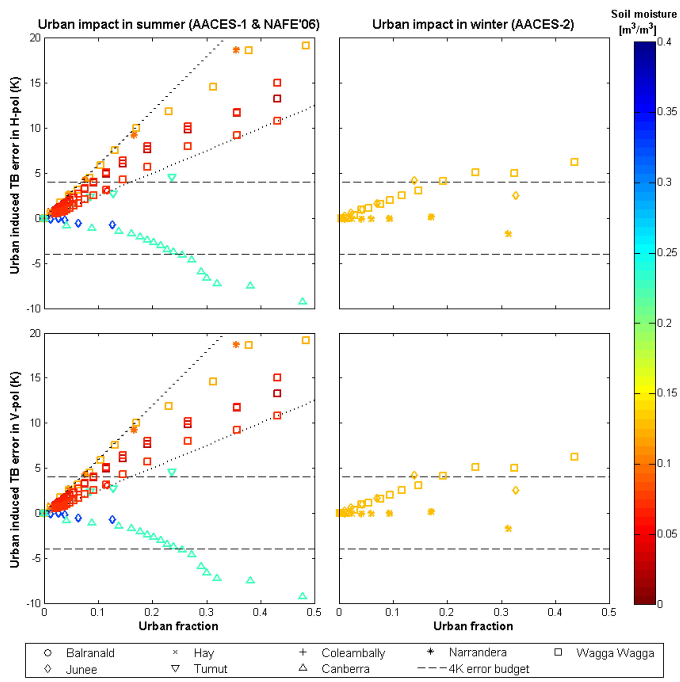

Fig. 5. Relationship between urban fraction and urban-induced brightness temperature error at 38.5° incidence angle for horizontal (top) and vertical (bottom) polarizations during summer (left) and winter (right) campaigns. Symbol color reflects the average soil moisture measurement collected using monitoring stations within the corresponding flight patch.

all pixels classified as urban, the assumption being that the surrounding brightness temperature response is representative of what would have been observed had the urban area not been there. The corresponding scene urban fraction $Frac_{\text{urban}}$ is also calculated.

This analysis was repeated for a total of 13 flights across the three airborne field experiments. In contradiction to the previous dry bare soil assumption on the microwave behavior of urban areas made in [16] and [23], the studied cities were observed to have a considerable (up to 50 K) lower brightness temperature than surrounding natural grass and cropping lands under most conditions. This phenomenon was also found from the airborne HUT-2D observations collected in December 2006 over the Porvoo area, Southern Finland [21]. A reasonable explanation is that the residential buildings usually having tile roofs are expected to behave like dry bare soil, while industrial buildings often having metal roofs have a very low emissivity and low physical temperature in early morning [21].

The urban-induced brightness temperature TB_{err} calculated from TB_{nonurban} and TB_{all} is plotted against $Frac_{\text{urban}}$ for summer and winter seasons separately in Fig. 5, with results coded by the average top ~5 cm soil moisture according to monitoring station measurements. As expected, the magnitude of TB_{err} increases as $Frac_{\text{urban}}$ is increased. During the summer campaigns (NAFE'06 and AACES-1), urban areas induced a positive TB_{err}, and the ratio between TB_{err} and $Frac_{\text{urban}}$ was shown to be dependent on the soil moisture condition, with a lower TB_{err} induced by urban area as the soil moisture increased. For soil moisture lower than 0.15 m^3/m^3, the brightness temperature difference between urban and urban-free areas was 25–60 K for horizontal polarization and 25–50 K for vertical polarization under warm summer conditions. Similar to urban effects under wet (soil moisture larger than 0.15 m^3/m^3) summer conditions, the impact of urban area was found to be much less in the winter campaign (AACES-2) than that under dry summer conditions. Due to a small soil moisture variation captured during the AACES-2, no clear relationship between TB_{err} and soil moisture was found.

One anomaly to the above results was for the airborne data collected over the city of Canberra on February 18, 2010. In this case, a negative relationship between TB_{err} and $Frac_{\text{urban}}$ was obtained; this flight was undertaken around 6 P.M. rather than at 6 A.M. This negative brightness temperature error has possibly resulted from two aspects. First, the ratio of industrial buildings drops from ~0.25 for the other studied cities to ~0.1 for Canberra, while the ratio of residential buildings increases from ~0.65 to ~0.9 (see Table II), thus the effective emissivity of man-made structures in Canberra is lower than the other studied cities. Second, the physical temperature of the urban area should be higher than that of the surrounding natural area in late afternoon due to urban heat island effect [49].

C. *Urban Cover Fraction Thresholds*

To meet the target soil moisture retrieval accuracy of SMOS and SMAP, their brightness temperature error budgets were used as benchmarks for urban contributions to brightness temperature that could be tolerated to still achieve the soil moisture retrieval accuracy target. Consequently, urban fraction thresholds for each mission were derived from the identical relationship shown in Fig. 5. Thus, urban fraction thresholds of 6.6% for horizontal polarization and 7.9% for vertical polarization were obtained for the SMOS 3.95-K error budgets under warm and dry conditions. Similarly, for the lower SMAP 1.3-K error budget, permissible urban fraction thresholds dropped to 2.2% and 2.6% for horizontal and vertical polarizations, respectively. Additionally, urban fraction thresholds of 16.8% and 5.2% were obtained for the SMOS and SMAP brightness temperature error budgets, respectively, under cold and/or wet conditions. For the purpose of simplicity, 6.6% and 16.8% were selected as urban fraction thresholds for the SMOS brightness temperature at both polarizations, under warm dry conditions and cold and/or wet conditions, respectively. These values reduce to 2.2% and 5.2% for the SMAP.

In comparison, the SMOS CATDS datasets have an urban fraction threshold of 10% to flag the presence of a limited urban area, and 30% to flag the presence of a large urban area [16]. In the SMAP *L2* datasets, an urban fraction threshold of 25% is used to flag for recommended quality and retrieve soil moisture [50].

D. *Urban Effects at Global Scale*

These urban fraction thresholds have been applied globally, together with the urban cover fraction maps, to identify where the

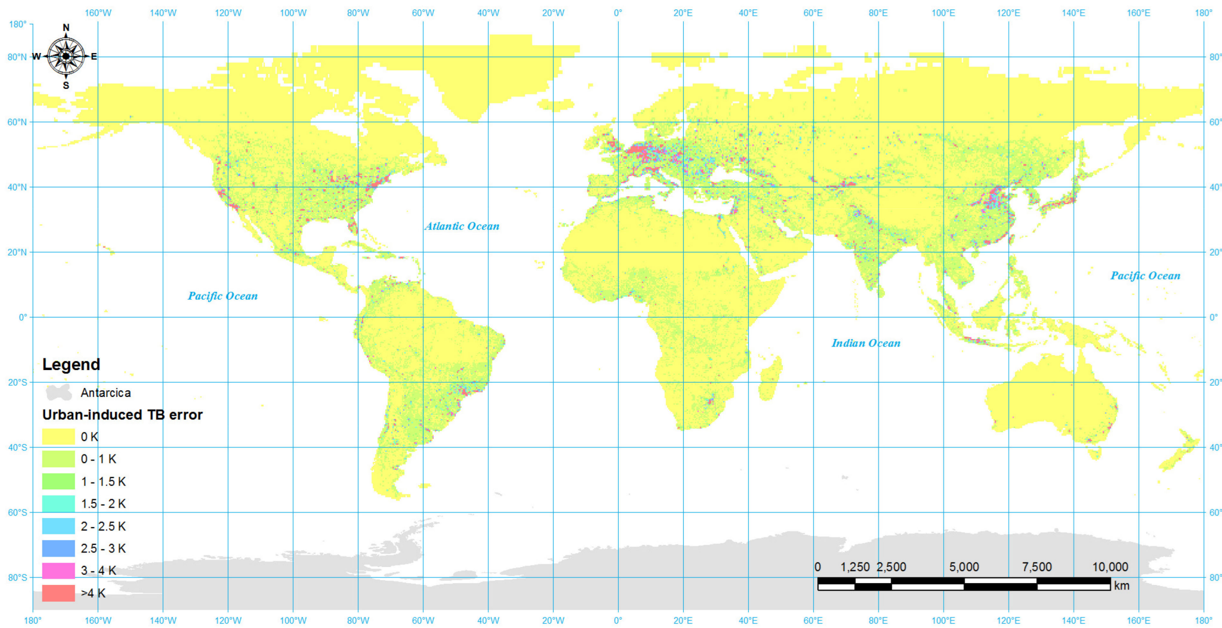

Fig. 6. Estimated maximum urban-induced brightness temperature error in the SMAP grid at global scale. Symbol color shows the level of brightness temperature error.

target soil moisture retrieval accuracy could be attained without explicitly accounting for man-made structures in the soil moisture retrieval algorithm. Consequently, the urban fraction at the SMOS and SMAP scales over the global land mass was calculated using the MODIS 500-m dataset. The urban land use raster of the MODIS 500-m dataset was converted to polygon format without any approximation or simplification, and then clipped with the SMOS DGG resampled 43-km circles and SMAP EASE 36-km pixels. The areal ratio between clipped area and the corresponding pixel is defined as the urban fraction of the given pixel.

Based on the relationship between the urban-induced brightness temperature "error" and urban fraction, the maximum brightness temperature error that would likely be introduced by ignoring the presence of urban was estimated from the calculated urban fraction of the SMOS and SMAP pixels. The maximum urban-induced errors over the globe are given in Fig. 6, showing that a brightness temperature error of more than 4 K may exist over highly urbanized areas such as Europe, East China, and the USA. Such brightness temperature contributions, if not accounted for, may subsequently yield soil moisture retrieval errors that exceed the target soil moisture retrieval accuracy when producing global soil moisture maps.

Fig. 7 shows the cumulative frequency curves of pixels that could be adversely affected for the SMOS and SMAP missions. Due to their similar scales, the SMOS and SMAP have similar cumulative distribution curves of urban fraction, but compared with their urban fraction thresholds approximated by their target radiometric calibration accuracy, there are about 2% of the SMOS pixels having urban-induced brightness temperature "error" in excess of the 3.95-K budget under warm dry conditions, reducing to ~0.5% under cold and/or wet conditions, while urban-induced brightness temperature error potentially exceeds the 1.3-K budget over ~5% SMAP pixels under warm dry conditions, and over ~2% SMAP pixels under cold and/or wet conditions. According to the distribution of urban impacted pixels of the SMOS (see Fig. 8) and SMAP (see Fig. 9), the urbanization ratio is not globally uniform and the area with higher density of urban area has more significant urban impact on soil moisture retrieval. The fraction of urban affected pixels was calculated for each individual continent and listed in Table IV. For more developed and populated areas, such as Europe, up to 4.5% of the SMOS and 14% of the SMAP pixels are likely to have urban-induced brightness temperature contributions in excess of their radiometric error budgets.

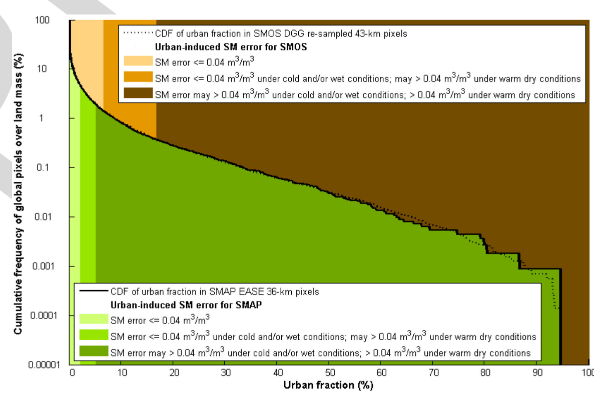

Fig. 7. CDFs of urban fraction of the SMOS (brown) and SMAP (green) pixels over land mass and the percentage of land pixels that is likely to be adversely affected by urban areas under different conditions.

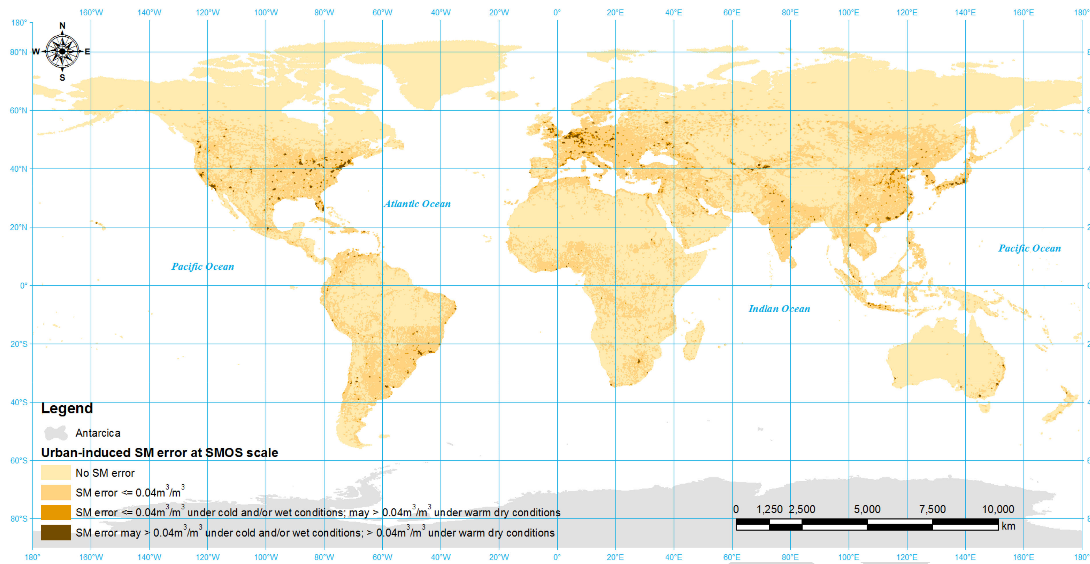

Fig. 8. Distribution of urban impacted pixels of SMOS over global land mass.

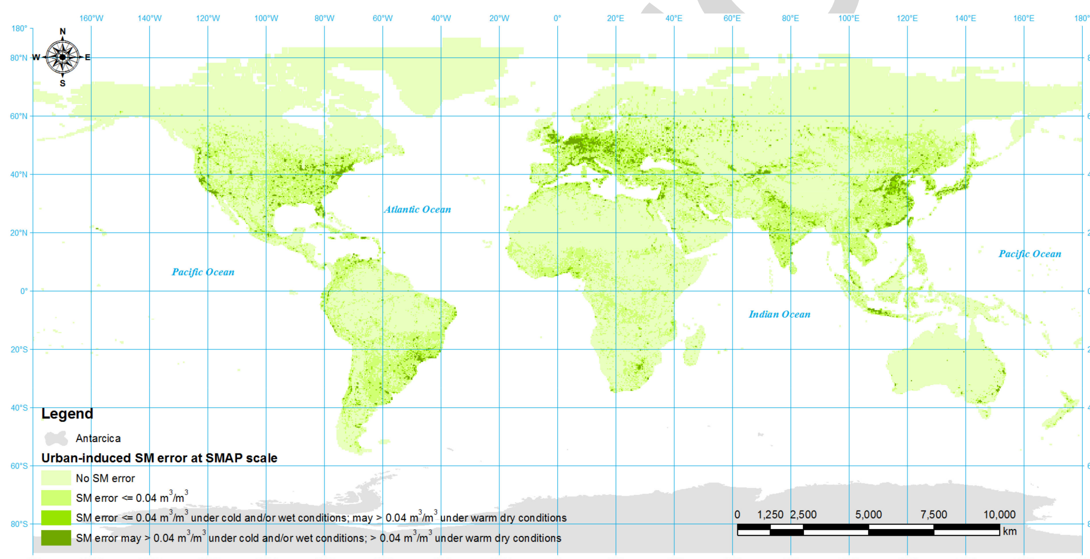

Fig. 9. Distribution of urban impacted pixels of SMAP over global land mass.

TABLE IV
STATISTICS OF URBAN IMPACT ON THE SMOS AND SMAP PIXELS

Urban-induced SM error	Urban fraction threshold for SMOS (SMAP) [%]	Fraction of the SMOS and (SMAP) pixels expected to exceed allowed brightness temperature error [%]						
		Africa	Asia	Europe	North America	Oceania	South America	Globe
No error	0.0 (0.0)	77.6 (78.8)	63.3 (64.8)	49.2 (52.5)	70.0 (72.4)	94.3 (94. 6)	58.6 (60.2)	67.8 (69.5)
Less than error budget	0.0 – 6.6 (0.0 – 2.2)	22.2 (20.0)	35.1 (29.9)	46.3 (33.5)	28.2 (23.5)	5.4 (4.4)	40.3 (35.5)	30.7 (26.0)
Less when cold and wet but more when warm and dry than error budget	6.6 – 16.8 (2.2 – 5.2)	0.2 (0.9)	1.3 (3.2)	3.4 (8.3)	1.1 (2.0)	0.2 (0.5)	0.9 (2.8)	1.1 (2.7)
More than error budget	> 16.8 (> 5.2)	0.1 (0.4)	0.3 (2.1)	1.1 (5.8)	0.7 (2.1)	0.2 (0.6)	0.3 (1.5)	0.4 (1.9)

V. Conclusion

Microwave radiometry has been widely acknowledged as the most promising technique to measure the spatial distribution of water content in the top ~5 cm soil layer, but the technique suffers from being a coarse resolution measurement of approximately 40 km. Consequently, the SMOS and SMAP soil moisture retrievals are at risk of being adversely affected by nonsoil targets, such as man-made structures in urban areas, in many parts of the world. Since only ~0.5% of the global land mass is urbanized, this is not expected to be a problem in most parts of the world, but urban areas are not uniformly distributed globally. Thus, it may not be possible to simply neglect the urban area effect, and so it is important to be able to flag or mask those pixels with nonnegligible urban-induced brightness temperature contributions, referred to here as an "error," in the absence of accounting for this contribution explicitly in the soil moisture retrieval process.

This study demonstrates the effect of urban area on the SMOS and SMAP brightness temperature observations using data acquired from the three airborne field experiments (NAFE'06, AACES-1, and AACES-2) conducted in the Murrumbidgee River Catchment, in South-Eastern Australia. The airborne brightness temperature observations at 1 km over seven medium-to-large cities were used together with the land use: NSW dataset on urban areas to establish the relationship between the urban-induced brightness temperature "error" and urban fraction. As expected, urban-induced brightness temperature error increased with urban fraction and was a function of soil moisture and temperature conditions. Moreover, a threshold of urban fraction was identified for the SMOS and SMAP based on their radiometric error budgets of 3.95 K and 1.3 K. Under warm dry (top ~5 cm soil moisture <0.15 m^3/m^3) conditions, the SMOS pixels with more than 6.6% urban fraction and the SMAP pixels with more than 2.2% urban fraction are expected to have urban-induced brightness temperature errors in excess of their radiometric error budgets. However, under cold and/or wet conditions the tolerance increases to 16.8% for the SMOS and 5.2% for the SMAP, respectively. Notably, these tolerances are much tighter than the 11%–20% tolerance suggested by earlier studies based on the model simulation.

Using these thresholds, the global SMOS and SMAP pixels expected to exhibit nonnegligible urban-induced brightness temperature error were identified, assuming similar microwave behaviors of the studied cities and urban areas in the other parts of the world. Using the MODIS 500-m global urban extent map, the urban fraction of the SMOS and SMAP pixels was calculated globally and the thresholds applied. Over land, approximately 2% of all the SMOS pixels may have significant urban-induced brightness temperature errors, reducing to about 0.5% of pixels under cold and/or wet conditions. Similarly, SMAP is expected to have up to 5% of pixels with significant urban-induced brightness temperature errors, reducing to about 2% under cold or wet conditions. The study also found that for more populated continents such as Europe, there may be as many as 14% of pixels that have significant urban-induced error. However, results have been extrapolated globally based on the microwave behaviors of only seven medium to large sized Australian cities, which may not be representative of the microwave response from urban areas elsewhere. Consequently, further studies of this nature should be conducted over different types of cities in other places of the world in order to validate the applicability of these results globally. Moreover, these results might be conservative as it has been assumed that the entire radiometric error budget can be attributed to urban-induced effects alone.

Acknowledgment

The authors would like to thank Prof. A. Schneider from the University of Wisconsin-Madison for providing access to MODIS urban land cover 500 m and Dr. N. Das and Dr. S. Chan from the California Institute of Technology for their constructive comments on this study. The airborne and ancillary ground data used in this paper were collected through earlier funding by the ARC and the goodwill of many volunteers during the NAFE and AACES field campaigns.

References

[1] D. Aubert, C. Loumagne, and L. Oudin, "Sequential assimilation of soil moisture and stream flow data in a conceptual rainfall—Runoff model," *J. Hydrol.*, vol. 280, no. 1, pp. 145–161, 2003.

[2] A. Olioso, H. Chauki, D. Courault, and J. P. Wigneron, "Estimation of evapotranspiration and photosynthesis by assimilation of remote sensing data into SVAT models," *Remote Sens. Environ.*, vol. 68, no. 3, pp. 341–356, 1999.

[3] J. Schnürer, M. Clarholm, S. Boström, and T. Rosswall, "Effects of moisture on soil microorganisms and nematodes: A field experiment," *Microbial Ecol.*, vol. 12, no. 2, pp. 217–230, 1986.

[4] R. A. de Jeu, T. R. Holmes, R. M. Parinussa, and M. Owe, "A spatially coherent global soil moisture product with improved temporal resolution," *J. Hydrol.*, vol. 516, pp. 284–296, 2014.

[5] W. T. Crow *et al.*, "Upscaling sparse ground-based soil moisture observations for the validation of coarse-resolution satellite soil moisture products," *Rev. Geophys.*, vol. 50, 2012, Art. no. RG2002

[6] D. Ryu and J. S. Famiglietti, "Characterization of footprint-scale surface soil moisture variability using Gaussian and beta distribution functions during the Southern Great Plains 1997 (SGP97) hydrology experiment," *Water Resour. Res.*, vol. 41, no. 12, 2005, Art. no. W12433.

[7] M. S. Yee, J. P. Walker, A. Monerris, C. Rüdiger, and T. J. Jackson, "On the identification of representative in situ soil moisture monitoring stations for the validation of SMAP soil moisture products in Australia," *J. Hydrol.*, vol. 537, pp. 367–381, 2016.

[8] G. Zucco, L. Brocca, T. Moramarco, and R. Morbidelli, "Influence of land use on soil moisture spatial–temporal variability and monitoring," *J. Hydrol.*, vol. 516, pp. 193–199, 2014.

[9] K. Rötzer, C. Montzka, and H. Vereecken, "Spatio-temporal variability of global soil moisture products," *J. Hydrol.*, vol. 522, pp. 187–202, 2015.

[10] L. Brocca, T. Tullo, F. Melone, T. Moramarco, and R. Morbidelli, "Catchment scale soil moisture spatial-temporal variability," *J. Hydrol.*, vol. 422, pp. 63–75, 2012.

[11] T. J. Jackson and T. J. Schmugge, "Passive microwave remote sensing system for soil moisture: Some supporting research," *IEEE Trans. Geosci. Remote Sens.*, vol. 27, no. 2, pp. 225–235, Mar. 1989.

[12] E. G. Njoku and D. Entekhabi, "Passive microwave remote sensing of soil moisture," *J. Hydrol.*, vol. 184, no. 1, pp. 101–129, 1996.

[13] E. G. Njoku *et al.*, "Observations of soil moisture using a passive and active low-frequency microwave airborne sensor during SGP99," *IEEE Trans. Geosci. Remote Sens.*, vol. 40, no. 12, pp. 2659–2673, Dec. 2002.

[14] T. Chen *et al.*, "Advantages of using microwave satellite soil moisture over gridded precipitation products and land surface model output in assessing regional vegetation water availability and growth dynamics for a lateral inflow receiving landscape," *Remote Sens.*, vol. 8, no. 5, 2016, Art. no. 428.

[15] Y. H. Kerr *et al.*, "The SMOS mission: New tool for monitoring key elements of the global water cycle," *Proc. IEEE*, vol. 98, no. 5, pp. 666–687, May 2010.

[16] Y. H. Kerr, P. Waldteufel, P. Richaume, I. Davenport, P. Ferrazzoli, and J.-P. Wigneron, "SMOS level 2 processor soil moisture algorithm theoretical basis document (ATBD)," SM-ESL (CBSA), CESBIO, Toulouse, France, SO-TN-ARR-L2PP-0037, no. 3/4, 2010.

[17] D. Entekhabi *et al.*, "The soil moisture active passive (SMAP) mission," *Proc. IEEE*, vol. 98, no. 5, pp. 704–716, May 2010.

[18] R. Oliva *et al.*, "SMOS radio frequency interference scenario: Status and actions taken to improve the RFI environment in the 1400–1427-MHz passive band," *IEEE Trans. Geosci. Remote Sens.*, vol. 50, no. 5, pp. 1427–1439, May 2012.

[19] J. R. Piepmeier *et al.*, "Radio-frequency interference mitigation for the soil moisture active passive microwave radiometer," *IEEE Trans. Geosci. Remote Sens.*, vol. 52, no. 1, pp. 761–775, Jan. 2014.

[20] P. N. Mohammed, M. Aksoy, J. R. Piepmeier, J. T. Johnson, and A. Bringer, "SMAP L-band microwave radiometer: RFI mitigation prelaunch analysis and first year on-orbit observations," *IEEE Trans. Geosci. Remote Sens.*, vol. 54, no. 10, pp. 6035–6047, Oct. 2016.

[21] K. Rautiainen, J. Kainulainen, T. Auer, J. Pihlflyckt, J. Kettunen, and M. T. Hallikainen, "Helsinki University of Technology L-band airborne synthetic aperture radiometer," *IEEE Trans. Geosci. Remote Sens.*, vol. 46, no. 3, pp. 717–726, Mar. 2008.

[22] A. Schneider, M. A. Friedl, and D. Potere, "Mapping global urban areas using MODIS 500-m data: New methods and datasets based on 'urban ecoregions'," *Remote Sens. Environ.*, vol. 114, no. 8, pp. 1733–1746, 2010.

[23] A. Loew, "Impact of surface heterogeneity on surface soil moisture retrievals from passive microwave data at the regional scale: The upper Danube case," *Remote Sens. Environ.*, vol. 112, no. 1, pp. 231–248, 2008.

[24] O. Merlin *et al.*, "The NAFE'06 data set: Towards soil moisture retrieval at intermediate resolution," *Adv. Water Resour.*, vol. 31, no. 11, pp. 1444–1455, 2008.

[25] S. Peischl *et al.*, "The AACES field experiments: SMOS calibration and validation across the Murrumbidgee river catchment," *Hydrol. Earth Syst. Sci.*, vol. 9, pp. 2763–2795, 2012.

[26] R. Panciera *et al.*, "The NAFE'05/CoSMOS data set: Toward SMOS soil moisture retrieval, downscaling, and assimilation," *IEEE Trans. Geosci. Remote Sens.*, vol. 46, no. 3, pp. 736–745, Mar. 2008.

[27] Australian Bureau of Statistics, "National regional profile 2006–2010," Nov. 1, 2011. [Online]. Available: http://www.ausstats.abs.gov.au/ausstats/nrpmaps.nsf/NEW+GmapPages/national+regional+profile

[28] B. Choudhury, T. Schmugge, and T. Mo, "A parameterization of effective soil temperature for microwave emission," *J. Geophys. Res.*, vol. 87, no. C2, pp. 1301–1304, 1982.

[29] A. B. Smith *et al.*, "The Murrumbidgee soil moisture monitoring network data set," *Water Resour. Res.*, vol. 48, no. 7, 2012, Art. no. W07701.

[30] E. Bartholomé and A. S. Belward, "GLC2000: A new approach to global land cover mapping from earth observation data," *Int. J. Remote Sens.*, vol. 26, no. 9, pp. 1959–1977, 2005.

[31] O. Arino *et al.*, "GlobCover: ESA service for global land cover from MERIS," in *Proc. IEEE Int. Geosci. Remote Sens. Symp.*, 2007, pp. 2412–2415.

[32] European Space Agency, "GlobCover products description validation report," Jul. 18, 2008. [Online]. Available: http://uranus.esrin.esa.int/pub/globcover_v2/global/GLOBCOVER_Products_Description_Validation_Report_I2.1.pdf

[33] Center for International Earth Science Information Network, "Global rural—Urban mapping project (GRUMP), alpha version: Urban extents," Jul. 18, 2004. [Online]. Available: http://sedac.ciesin.columbia.edu/gpw

[34] C. D. Elvidge *et al.*, "Global distribution and density of constructed impervious surfaces," *Sensors*, vol. 7, no. 9, pp. 1962–1979, 2007.

[35] A. Schneider, M. A. Friedl, and C. E. Woodcock, "Mapping urban areas by fusing multiple sources of coarse resolution remotely sensed data," in *Proc. IEEE Int. Geosci. Remote Sens. Symp.*, 2003, vol. 4, pp. 2623–2625.

[36] K. K. Goldewijk, "Estimating global land use change over the past 300 years: The HYDE database," *Global Biogeochem. Cycles*, vol. 15, no. 2, pp. 417–433, 2001.

[37] K. K. Goldewijk, "Three centuries of global population growth: A spatial referenced population (density) database for 1700–2000," *Population Environ.*, vol. 26, no. 4, pp. 343–367, 2005.

[38] D. M. Danko, "The digital chart of the world project," *Photogramm. Eng. Remote Sens.*, vol. 58, no. 8, pp. 1125–1128, 1992.

[39] C. D. Elvidge *et al.*, "Night-time lights of the world: 1994–1995," *ISPRS J. Photogramm. Remote Sens.*, vol. 56, no. 2, pp. 81–99, 2001.

[40] M. L. Imhoff, W. T. Lawrence, D. C. Stutzer, and C. D. Elvidge, "A technique for using composite DMSP/OLS "city lights" satellite data to map urban area," *Remote Sens. Environ.*, vol. 61, no. 3, pp. 361–370, 1997.

[41] B. Bhaduri, E. Bright, P. Coleman, and J. Dobson, "LandScan," *Geoinformatics*, vol. 5, no. 2, pp. 34–37, 2002.

[42] N. Ye, J. P. Walker, and C. Rüdiger, "A cumulative distribution function method for normalizing variable-angle microwave observations," *IEEE Trans. Geosci. Remote Sens.*, vol. 53, no. 7, pp. 3906–3916, Jul. 2015.

[43] "Metadata statement: Land use mapping," New South Wales Dept. Environ. Climate Change, Hurstville, NSW, Australia, Jul. 17, 2007. [Online]. Available: http://www.canri.nsw.gov.au/download/NSW_Land_Use_Mapping_metadata.pdf

[44] D. Potere and A. Schneider, "A critical look at representations of urban areas in global maps," *GeoJournal*, vol. 69, no. 1/2, pp. 55–80, 2007.

[45] D. Potere, A. Schneider, S. Angel, and D. L. Civco, "Mapping urban areas on a global scale: Which of the eight maps now available is more accurate?" *Int. J. Remote Sens.*, vol. 30, no. 24, pp. 6531–6558, 2009.

[46] R. Panciera, J. P. Walker, E. Kim, J. Kalma, and O. Merlin, "Effect of spatial scale on soil moisture retrieval from passive microwave sensors," presented at the MODSIM Int. Congr. Model. Simul., Dec. 2007.

[47] K. Sahr, D. White, and A. J. Kimerling, "Geodesic discrete global grid systems," *Cartogr. Geograph. Inf. Sci.*, vol. 30, no. 2, pp. 121–134, 2003.

[48] M. J. Brodzik, B. Billingsley, T. Haran, B. Raup, and M. H. Savoie, "EASE-grid 2.0: Incremental but significant improvements for earth-gridded data sets," *ISPRS Int. J. Geo-Inf.*, vol. 1, no. 1, pp. 32–45, 2012.

[49] A. M. Rizwan, L. Y. Dennis, and L. Chunho, "A review on the generation, determination and mitigation of urban heat island," *J. Environ. Sci.*, vol. 20, no. 1, pp. 120–128, 2008.

[50] P. O'Neill, R. Bindlish, S. Chan, E. Njoku, and T. Jackson, "Algorithm theoretical basis document level 2 & 3 soil moisture (passive) data products," Jet Propul. Lab., California Inst. Technol., Pasadena, CA, USA, vol. Revision D, Jun. 6, 2018.

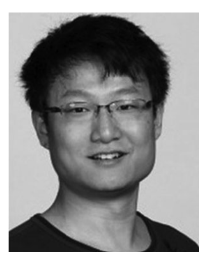

Nan Ye received the B.E. degree in hydraulic and hydropower engineering from Tsinghua University, Beijing, China, in 2006, and the Ph.D. degree in civil engineering from Monash University, Melbourne, VIC, Australia, in 2014.

He then coordinated a number of airborne field experiments for the in-orbit calibration/validation of the soil moisture active passive mission in the Murrumbidgee River catchment, southeast of Australia. He is currently a Senior Research Fellow with Monash University working on *P*-band passive microwave remote sensing of soil moisture.

Jeffrey P. Walker (M'13–F'xx) received the B.E. degree in civil engineering and the Bachelor of Surveying (Hons. 1 and University Medal) degree from the University of Newcastle, Callaghan, NSW, Australia, in 1995, and the Ph.D. degree in water resources engineering from the University of Newcastle in 1999.

He then joined the NASA Goddard Space Flight Centre to implement his soil moisture work globally. In 2001, he was a Lecturer with the Department of Civil and Environmental Engineering, University of Melbourne, Melbourne, VIC, Australia. Since 2010, he has been a Professor with the Department of Civil Engineering, Monash University, Melbourne, where he is continuing his research. He is contributing to soil moisture satellite missions at NASA, ESA, and JAXA, as a Science Team Member for the soil moisture active passive mission and Cal/Val Team Member for the soil moisture and ocean salinity and global change observation mission—water, respectively.

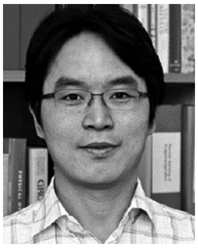

Dongryeol Ryu (M'05) received the B.S. and M.S. degrees in geology from Seoul National University, Seoul, South Korea, in 1997 and 2000, respectively, and the Ph.D. degree in earth system science from the University of California, Irvine, CA, USA, in 2006.

He is currently an Associate Professor with the Department of Infrastructure Engineering, Melbourne School of Engineering, University of Melbourne, Melbourne, VIC, Australia. His research interests include hydrological modeling, remote sensing of land surface variables such as soil moisture and vegetation characteristics, their spatial and temporal variability, and hydrologic application of the remotely sensed land surface properties.

Robert J. Gurney was the Head of the Hydrological Sciences Branch, NASA Goddard Space Flight Centre, Greenbelt, MD, USA, where he was also the Director of the Environmental Systems Science Centre for 18 years. He is currently a Professor of Earth Observation Science with the University of Reading, Reading, U.K. He has recently jointly chaired the data and information systems collaborative research action of the Belmont Forum to further this aim. His research interests include the use of remote sensing to understand hydrological processes at the land surface and bringing together multiple datasets to understand the earth system.